Experimental Evidence of Hydrodynamic Instantons:
The Universal Route to Rogue Waves

Giovanni Dematteis,[1, 2] Tobias Grafke,[3] Miguel Onorato,[2, 4] and Eric Vanden-Eijnden[5]

[1]*Dipartimento di Scienze Matematiche, Politecnico di Torino,*
Corso Duca degli Abruzzi 24, I-10129 Torino, Italy
[2]*Dipartimento di Fisica, Università degli Studi di Torino, Via Pietro Giuria 1, 10125 Torino, Italy*
[3]*Mathematics Institute, University of Warwick, Coventry CV4 7AL, United Kingdom*
[4]*INFN, Sezione di Torino, Via Pietro Giuria 1, 10125 Torino, Italy*
[5]*Courant Institute, New York University, 251 Mercer Street, New York, NY 10012, USA*
(Dated: November 7, 2019)

A statistical theory of rogue waves is proposed and tested against experimental data collected in a long water tank where random waves with different degrees of nonlinearity are mechanically generated and free to propagate along the flume. Strong evidence is given that the rogue waves observed in the tank are *hydrodynamic instantons*, that is, saddle point configurations of the action associated with the stochastic model of the wave system. As shown here, these hydrodynamic instantons are complex spatio-temporal wave field configurations which can be defined using the mathematical framework of Large Deviation Theory and calculated via tailored numerical methods. These results indicate that the instantons describe equally well rogue waves that originate from a simple linear superposition mechanism (in weakly nonlinear conditions) or from a nonlinear focusing one (in strongly nonlinear conditions), paving the way for the development of a unified explanation to rogue wave formation.

I. INTRODUCTION

A fascinating phenomenon observed in a wide class of nonlinear dispersive systems is the occurrence of rogue waves with abnormally large amplitude; they are found in sea surface gravity waves [1, 2], nonlinear fiber optics [3], plasmas [4] and Bose-Einstein condensates. Rogue waves have received a lot of attention in the past 20 years, and different mechanisms for their formation have been put forward, but a definite explanation has yet to be agreed upon [2, 5–9]. To settle this question, studies in wave flumes or basins are interesting, because they permit to create and measure wave states by means of mechanical wave generators under controlled conditions meant to mimic (after rescaling) those in the sea. The water surface in the tank can be monitored accurately with high space-time resolution, and abundant statistics can be collected. In one-dimensional experiments that mimic an idealized long-crested rescaled sea, if the surface is sufficiently energetic, nonlinear focusing effects take over linear dispersion and are known to be responsible for increasing the likelihood of the rogue waves. This leads to non-Gaussian fat-tailed statistics for their amplitude [2, 10], as opposed to the Gaussian statistics observed in the dispersive regime.

In the present article, we propose a statistical theory of rogue waves and test it against experiments performed in the one-dimensional setting of the wave flume. We show that, in the full range of experimental conditions tested, the rogue waves we observe closely resemble *hydrodynamic instantons* [11–16]: these are specific spatio-temporal configurations of the wave field which we define within the framework of large deviation theory (LDT) as the minimizers of an action associated with the random wave model used to describe the system; here we fo-

cus on the nonlinear Schrödinger equation (NLSE) with random initial data but the approach is generalizable to more complicated models. The finding that instantons explain experimental rogue waves for a wide range of surface conditions in the tank is striking because it offers a unified description of these waves. In particular, our approach encompasses two of the main existing theories for rogue wave creation: (i) the *theory of quasi-determinism* [17, 18] which predicts that the rogue wave is created by linear superposition effects and its shape is given by the autocorrelation function of the wave field; (ii) the *semi-classical theory* [19, 20] which asserts instead that localized perturbations in the wave field can lead to the formation of a Peregrine soliton via nonlinear focusing instability. Our approach reconciles these two, apparently incompatible, theories and smoothly interpolates between them as the experimental control parameters are varied: when the nonlinear effects are weak, the shape of the instantons converges to the autocorrelation function predicted by the theory of quasi-determinism; and when the nonlinear effects are strong, their shape converges to that of the Peregrine soliton. Because the instanton calculus proposed in this paper uses as limiting parameter the maximal wave amplitude itself, without condition on model parameters or regimes in NLSE, it allows us to assess the validity of the quasi-deterministic and semi-classical theories by comparing them to the results of our approach in appropriate regimes. Our approach could also be useful in the context of other nonlinear theories for rogue waves based on NLSE, like statistical approaches based on the Alber and the Wigner equations [35, 37–41]. We also stress that the method proposed here can be generalized to the full two-dimensional setting, as well as other relevant physical systems where an understanding of extreme events is important [21, 22]

but made challenging by the complexity of the models involved combined with the stochasticity of their evolution and the uncertainty of their parameters [21, 23–26]. In this sense our approach adds to other rare events methods [27–34].

The remainder of this paper is organized as follows: We introduce the experimental setup in section II. In section III, we explain how we extract extreme event data from the experimental measurements. Our approach based on large deviation theory is presented in Sec. IV, where we also describe how we compute the instanton for the rogue waves. Theory and experiment are then compared in section V, with special focus on the quasi-linear and highly nonlinear limiting cases. We conclude in section VI by discussing the implications of our results in the context of a unified theory of rogue waves.

II. EXPERIMENTAL SETUP

The experimental data were recorded in the 270m long wave flume at Marintek (Norway) [36, 42], schematically represented in Fig. 1. At one end of the tank a plane-wave generator perturbs the water surface with a predefined random signal. These perturbations create long-crested wave trains that propagate along the tank toward the opposite end, where they eventually break on a smooth beach that suppresses most of the reflections. The water surface $\eta(x,t)$ is measured by probes placed at different distances from the wave maker (x-coordinate). The signal at the wave maker $\eta(x = 0, t) \equiv \eta_0(t)$ is prepared according to the stationary random-phase statistics with deterministic spectral amplitudes $C(\omega_j)$:

$$\eta_0^e(t) = \sum_{j=1}^{N} \sqrt{2C(\omega_j)\delta\omega} \cos(\omega_j t + \phi_j). \qquad (1)$$

Here the phases ϕ_j's are mutually independent random variables uniformly distributed on $[0, 2\pi]$, $\delta\omega = \frac{2\pi}{\tau}$, $\omega_j = j\delta\omega$, and τ is the time-series length. This guarantees that, for N and τ sufficiently large, $\eta_0^e(t)$ is approximately a stationary Gaussian random field with energy spectrum $C(\omega) > 0$, i.e.

$$\langle \eta_0^e(t)\eta_0^e(t') \rangle = \sum_{j=1}^{N} C(\omega_j)\delta\omega \cos(\omega_j(t - t')) \qquad (2)$$
$$\sim \int_0^\infty C(\omega) \cos(\omega(t - t'))d\omega,$$

where the bracket denotes expectation with respect to the random phases ϕ_j. In the experiment, $C(\omega)$ is taken to be the JONSWAP spectrum [43] of deep water waves observed in the ocean,

$$C(\omega) = \frac{\alpha g^2}{\omega^5} \exp\left[-\frac{5}{4}\left(\frac{\omega_0}{\omega}\right)^4\right] \gamma^{\exp\left[-\frac{(\omega-\omega_0)^2}{2\sigma_J^2\omega_0^2}\right]}. \qquad (3)$$

Here $g = 9.81\text{ms}^{-2}$ is the gravity acceleration, $\omega_0 = 4.19$ s^{-1} is the carrier frequency (spectral peak), and $\sigma_J = 0.07$

if $\omega \leq \omega_0$ and $\sigma_J = 0.09$ if $\omega > \omega_0$. These parameters are fixed for all sea states, and we can use the dispersion relation of surface gravity waves in deep water to obtain the carrier wave number $k_0 = \omega_0^2/g = 1.79$ m^{-1}. The remaining parameters α and γ in (3) are dimensionless and vary according to weather conditions. In the experiments, $\alpha = 0.012$ throughout, while the enhancement factor γ ranges from 1 to 6, which is a realistic range of values for the ocean measurements from calmer to rougher sea states. In the water waves community, it is common to introduce the significant wave height H_s, as a statistical measure of the average wave height, here defined as

$$H_s = 4\sigma = 4\left(\int_0^\infty C(\omega)d\omega\right)^{1/2}, \qquad (4)$$

where $\sigma = \langle \eta_0^2 \rangle^{1/2}$ is the standard deviation of the surface elevation, which both depend on γ as well as the other parameters in (3) that we keep fixed as specified above. We also introduce a characteristic bandwidth Ω of the JONSWAP spectrum defined as

$$\Omega = \text{width of } C(\omega) \text{ at half height.} \qquad (5)$$

Experimental data were collected for three different regimes: *quasi-linear* ($\gamma = 1$, $H_s = 0.11$ m), *intermediate* ($\gamma = 3.3$, $H_s = 0.13$ m), and *highly nonlinear* ($\gamma = 6$, $H_s = 0.15$ m), see Table I. Note that these three regimes have comparable significant wave heights H_s, but the difference in their enhancement factors γ has significant dynamical consequences, as discussed in Sec. IV where we introduce and explain the additional parameters ϵ, L_{lin}, and L_{Per} listed in the table. Experimental measurements of the spectrum for the three regimes are depicted in Fig. 2.

For each set, we use data from 5 time series, each of which is 25 min long. The surface elevation η is measured simultaneously by 19 probes placed at different locations along the axes at the center of the tank, recording data with a rate of 40 measurements per second. At each of two different positions ($x = 75$ m and $x = 160$ m) two extra probes closer to the sides are used to check that the wave fronts remain planar.

III. EXTREME-EVENT FILTERING: EXTRACTING ROGUE WAVES FROM EXPERIMENTAL DATA

To characterize the dynamics leading to extreme events of the water surface, we adopt the following procedure: at a fixed location $x = L$ along the flume, we select small observation windows around all temporal maxima of η that exceed a threshold z. The choice of the threshold z is meant to select extreme events with a similar probability for all sets: the values of $z = H_s = 4\sigma$ for the quasi-linear set, $z = 1.1\,H_s = 4.4\sigma$ for the intermediate set and $z = 1.2\,H_s = 4.8\sigma$ for the highly-nonlinear set lead
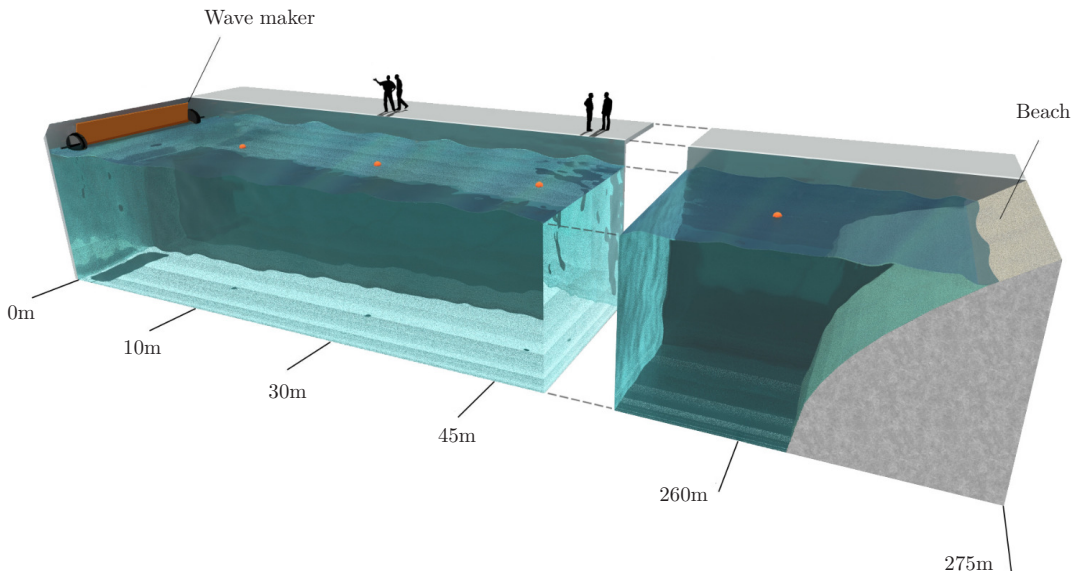
FIG. 1. *Wave flume experiment.* The wave maker generates a random wave field with stationary Gaussian statistics with the JONSWAP energy spectrum observed in the oceans. The planar wave fronts propagate along the water tank, where the surface elevation η is measured by vertical probes.
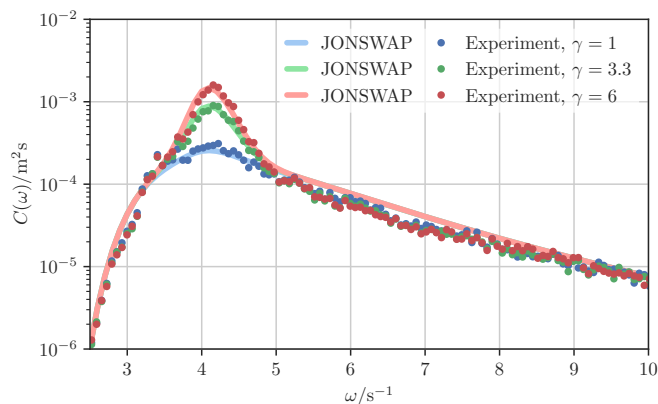

FIG. 2. JONSWAP spectra from Eq. (3) for the three experimental regimes of table I (lines), compared to experimental measurements at the $x = 10$m probe (dots). These spectra remain roughly constant through the tank, except for small changes that are the signature of non-Gaussian effects that develop [42].

Regime	γ	$H_s(\mathrm{m})$	$\Omega(\mathrm{s}^{-1})$	ϵ	$L_{\mathrm{lin}}(\mathrm{m})$	$L_{\mathrm{Per}}(\mathrm{m})$
quasi-linear	1	0.11	2.12	0.15	8.9	32
intermediate	3.3	0.13	0.90	1.13	46	61
highly nonlinear	6	0.15	0.76	2.23	69	65

TABLE I. The relevant parameters in the three experimental regimes considered. The parameters γ, H_s, and Ω are used to characterize the JONSWAP spectrum enforced by the wave maker. The parameter ϵ is used to quantify the strength of nonlinear versus dispersive effects in NLSE and is defined in Sec. IV A. The two lengths L_{lin} and L_{Per} measure the typical scales over which these effects occur: they are defined in Section V C and are useful for the interpretation of Fig. 6 .

respectively to 78, 99 and 88 registered events where the maximum of the surface elevation exceeds the threshold at the 45 m probe, $\eta(x = 45 \text{ m}, t) \geq z$. We track the wave packet backward in space and look at its shape at earlier points in the channel. This allows us to build a collection of extreme events and monitor their precursors. In Fig. 3a, we show two extreme events at $x = 45$ m obtained by this procedure, as well as their precursors at $x = 30$ m and $x = 10$ m. We analyze the statistical properties of these extreme events by computing their average shape and the standard deviation around it at the different po-

sitions along the channel, obtaining the result shown in Fig. 3b for the highly-nonlinear case.

IV. THEORETICAL DESCRIPTION OF ROGUE WAVES VIA INSTANTONS OF NLSE

We now explain how rogue waves can, within the framework of Large Deviation, be described as instantons, that is, the minimizers of an action functional associated with the nonlinear Schrödinger equation with random initial data that we will use to describe the system's evolution. In the linear case, as will be discussed later, this minimization can be done analytically without much effort. When the nonlinear effects matter, however, numerical computations are required to perform the minimization.
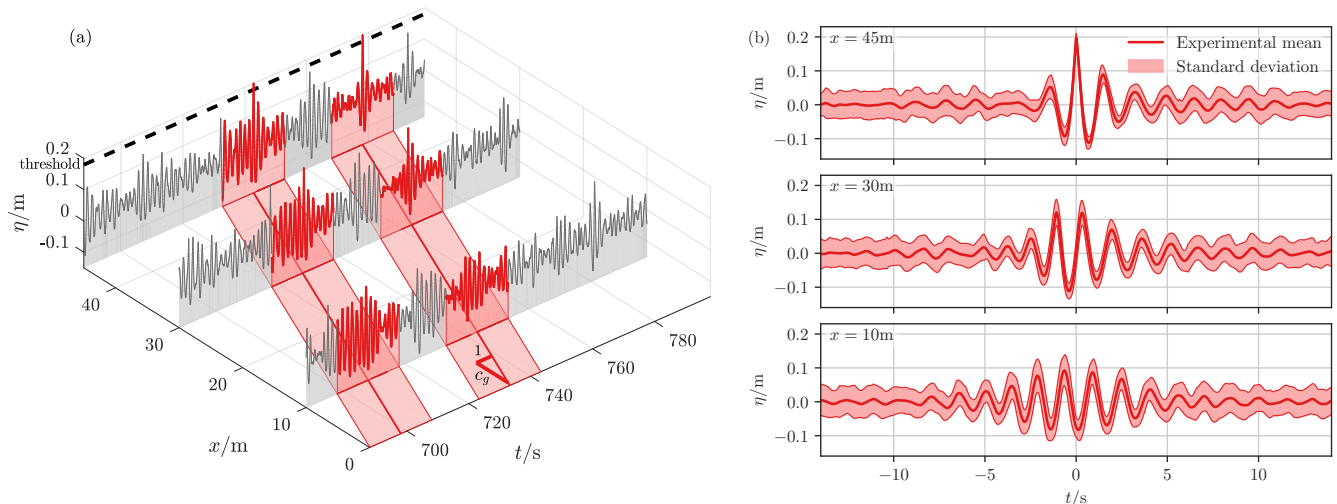
FIG. 3. (a) *Extreme wave event selection*. At $x = 45$ m, we monitor the temporal maximum of the experimental data series of η, record events reaching above a given threshold, and monitor the evolution of these events at probes located earlier in the channel. This is done within an observation time window centered at the maximum and following the wave packet with group velocity c_g; we repeat this for the whole time series to build a collection of extreme events and their evolution. (b) *Mean extreme event*. The thick line shows the mean extreme event at different points along the channel, the shaded area a 1 standard deviation range around it. The *noise to signal* ratio is small in the focusing region, leading naturally to the question: Can we explain the common pathway by which these rogue waves are most likely to arise?

A. The model

To avoid solving fully nonlinear water wave equations that are complicated from both theoretical and computational viewpoints, it is customary to use simplified models such as the Nonlinear Schrödinger equation (NLSE). If we exclude very nonlinear initial data, it is known that NLSE captures the statistical properties of one dimensional wave propagation to a good degree of accuracy up to a certain time [1, 2, 10, 45–47] and it can be improved upon by using higher order envelope equations [48, 49]. Because of their simplicity, NLSE and extensions thereof have been successfully used to explain basics mechanisms such as the modulational instability in water waves. With the aim of capturing leading order effects, rather than describing the full wave dynamics, here we restrict ourselves to the NLSE as a prototype model for describing the nonlinear and dispersive waves in the wave flume. Higher order models could in principle improve the agreement between the theoretical instantons and the experimental ones, but as demonstrated later, these corrections are negligible in the wave flume experiment.

In the limit of *deep-water*, *small-steepness*, and *narrow-band* properties, the evolution of the system is described, to leading order in nonlinearity and dispersion, by the one-dimensional NLSE:

$$\frac{\partial \psi}{\partial x} + 2\frac{k_0}{\omega_0}\frac{\partial \psi}{\partial t} + i\frac{k_0}{\omega_0^2}\frac{\partial^2 \psi}{\partial t^2} + 2ik_0^3|\psi|^2\psi = 0. \quad (6)$$

The NLSE describes the change of the complex enve-

lope $\psi \equiv \psi(x,t)$ that relates to the surface elevation via the Stokes series truncated at second order:

$$\eta = |\psi|\cos(\theta) + \tfrac{1}{2}k_0|\psi|^2\cos(2\theta) + O(k_0^2|\psi|^3), \quad (7)$$

where $\theta = k_0 x - \omega_0 t + \beta$ and β is the phase of ψ. In this expression the second order term can be neglected when the field amplitude $|\psi|$ is small—this is the case near the wave maker at $x = 0$, where we will specify initial conditions for the NLSE (6). However, this second order correction is important when $|\psi|$ becomes large, i.e. when rogue waves develop.

The NLSE (6) is written as an evolution equation in space (rather than in time) in order to facilitate the comparison with experimental data which are taken along the spatial extend of the flume. Consistent with the wave generator located at $x = 0$, we specify $\psi(x = 0, t) = \psi_0(t)$ as initial condition for (7), which we take to be a Gaussian random field with a covariance whose Fourier transform is related to the JONSWAP spectrum (3). Specifically, we set

$$\psi_0(t) = \int_{-\infty}^{\infty} e^{i\omega t}\hat{\psi}_0(\omega)d\omega \quad (8)$$

with $\hat{\psi}_0(\omega)$ Gaussian with mean zero and covariance

$$\langle \hat{\psi}_0(\omega)\bar{\hat{\psi}}_0(\omega')\rangle = C(\omega - \omega_0)\delta(\omega - \omega')$$
$$\langle \hat{\psi}_0(\omega)\hat{\psi}_0(\omega')\rangle = \langle \bar{\hat{\psi}}_0(\omega)\bar{\hat{\psi}}_0(\omega')\rangle = 0 \quad (9)$$

where the bar denotes complex conjugation and $C(\omega) = C(-\omega)$ is the JONSWAP spectrum defined in (3). Since,

to first order,

$$\eta_0(t) = \tfrac{1}{2}\left(\psi_0(t)e^{-i\omega_0 t} + \bar{\psi}_0(t)e^{i\omega_0 t}\right) + O(k_0|\psi_0|^2) \quad (10)$$

a direct calculation reported in Appendix A shows that, to that order, $\eta_0(t)$ is Gaussian with mean zero and co-variance $C(\omega)$. Note that in our setup the initial $\psi_0(t)$ is the only source of randomness in the model. That is, we evolve $\psi_0(t)$ in space by the NLSE, and look for solutions $\psi(x,t)$ whose elevation $\eta(x,t)$ exceed the threshold z at spatial position $x = L$, i.e. satisfy $\eta(L,t) \geq z$ for some $t \geq 0$ (using temporal invariance we will later designate $t = 0$ to be the point in time of the extreme event).

The NLSE (6) is Hamilton's equation $i\left(\partial_x + (2k_0/\omega_0)\partial_t\right)\psi = \delta H/\delta\bar{\psi}$ associated with the Hamiltonian $H = H_{\mathrm{lin}} + H_{\mathrm{nl}}$, with

$$H_{\mathrm{lin}} = -\frac{k_0}{\omega_0^2}\int_{-\infty}^{\infty}|\partial_t\psi|^2 dt, \quad H_{\mathrm{nl}} = k_0^3\int_{-\infty}^{\infty}|\psi|^4 dt. \quad (11)$$

In order to quantify the magnitude of the nonlinearity of the wavefield, we use the ratio ϵ between the nonlinear energy H_{nl} and the free particle linear energy H_{lin}. To this end, we use dimensional analysis to estimate $|\partial_t\psi|^2 = O(\Omega^2 H_s^2)$ and $|\psi|^4 = O(H_s^4)$, where averaged wave height H_s and the characteristic frequency Ω are defined in (4) and (5), respectively . This gives

$$\epsilon = \frac{H_{\mathrm{nl}}}{H_{\mathrm{lin}}} = \left(\frac{\omega_0}{\Omega}k_0 H_s\right)^2. \quad (12)$$

The values of ϵ obtained this way are given in Table I for the three regimes analyzed: quasi-linear, intermediate, and highly nonlinear. We stress that other definitions of the nonlinearity parameter are possible, differing by a constant factor—the important information is the relative magnitude of ϵ in the different regimes. We also stress that the values of ϵ are used to interpret the results, but the instanton calculations described next in Sec. IV B are performed in the same way for all values of ϵ.

B. Large Deviation Theory and Instanton Calculus

Our analytical and computational descriptions of rare events rely on *instanton theory*. Developed originally in the context of quantum chromodynamics [13], at its core lies the realization that the evolution of any stochastic system, be it quantum and classical, reduces to a well-defined (semi-classical) limit in the presence of a small parameter. Concretely, the simultaneous evaluation of all possible realizations of the system subject to a given constraint results in a (classical or path-) integral whose integrand contains an action functional $S(\psi)$. The dominating realization can then be obtained by approximating the integral by its *saddle point approximation*, using the solution to $\delta S(\psi^*)/\delta\psi = 0$. This critical point ψ^* of the action functional is called the *instanton*, and it yields the

maximum likelihood realization of the event. This conclusion can also be justified mathematically within Large Deviation Theory.

Specifically, we are interested in the probability

$$P_L(z) \equiv \mathbb{P}(\eta(L,0) \geq z) \quad (13)$$

i.e. the probability of the surface elevation at position L at an arbitrary time $t = 0$ exceeding a threshold z. This probability can in principle be obtained by integrating the distribution of the initial conditions over the set

$$\Lambda(z) = \{\psi_0 : \eta(L,0)) \geq z\}, \quad (14)$$

i.e. the set of all initial conditions ψ_0 at the wave maker $x = 0$ that exceed the threshold z further down the flume at $x = L$. Since the initial field $\psi_0(t)$ is Gaussian, consistent with (9) the probability (13) can therefore be formally written as the path integral

$$P_L(z) = Z^{-1}\int_{\Lambda(z)}\exp\left(-\tfrac{1}{2}\|\psi_0\|_C^2\right)D[\psi_0], \quad (15)$$

where Z is a normalization constant and we defined

$$\|\psi_0\|_C^2 = \int_{-\infty}^{\infty}\frac{|\hat{\psi}_0(\omega)|^2}{C(\omega - \omega_0)}d\omega \quad (16)$$

where $\hat{\psi}_0(\omega) = 1/(2\pi)\int_{-\infty}^{\infty}\psi_0(t)e^{-i\omega t}dt$ is the Fourier transform of $\psi_0(t)$. The functional integral (15) can be given a precise mathematical meaning in several ways. For example, we can project the initial field onto finitely many modes, in which case (15) reduces to a regular integral over these modes. However, even if we were to perform this projection, the integration is hard to perform in practice. This is because the set $\Lambda(z)$ defined in (14) has a very complicated shape in general, that depends non-trivially on the nonlinear dynamics of (6) since it involves the field at $x = L > 0$ down the flume rather than $x = 0$. One way around this difficulty is to estimate the integral (15) via Laplace's method. This strategy is the essence of *Large deviation theory* (LDT), or, equivalently, *instanton calculus*, and it is justified for large z, when the probability of the set $\Lambda(z)$ is dominated by a single ψ_0 contributing most to the integral (see [26, 50]). The optimal condition leads to the constrained minimization problem

$$\tfrac{1}{2}\min_{\psi_0\in\Lambda(z)}\|\psi_0\|_C^2 \equiv I_L(z), \quad (17)$$

and gives the large deviation estimate for Eq. (13),

$$P_L(z) \asymp \exp\left(-I_L(z)\right). \quad (18)$$

where the symbol $\asymp$ means asymptotic logarithmic equivalence, i.e. the ratio of the logarithms of the two sides tends to 1 as $z \to \infty$, or, in other words, the exponential portion of both sides scales in the same way with z. Intuitively, the estimate (18) says that, in the limit of extremely strong (and unlikely) waves, their probability

is dominated by their least unlikely realization, the instanton.

In practice, the constraint $\eta(L,0) \geq z$ can be imposed by adding a Lagrange multiplier term to Eq. (17), and it is easier to use this multiplier as control parameter and simply see *a posteriori* what value of z it implies. Concretely, we perform for various values of λ the minimization

$$\min_{\psi_0} \left(\tfrac{1}{2} \|\psi_0\|_C^2 - \lambda \eta(L,0) \right) \equiv S_L(\lambda), \qquad (19)$$

over all the possible realizations of ψ_0 (without constraint). The minimizer $\psi_0^\star(\lambda)$ of this optimization problem gives the following parametric representation of $I_L(z)$ versus z:

$$
\begin{aligned}
I_L(z(\lambda)) &= \tfrac{1}{2} \|\psi_0^\star(\lambda)\|_C^2, \\
z(\lambda) &= \eta(L,0) = |\psi(L,0)| \left(1 + \tfrac{1}{2} k_0 |\psi(L,0)| \right),
\end{aligned}
\qquad (20)
$$

where the last equivalence uses the second order of the Stokes' series (7) at $\theta = 0$. It is easy to see from Eqs. (17) and (19) that $S_L(\lambda)$ is the Legendre transform of $I_L(z)$ since:

$$
\begin{aligned}
S_L(\lambda) &= \sup_{z \in \mathbb{R}} (\lambda z - I_L(z)) \\
&= \sup_{z \in \mathbb{R}} (\lambda z - \tfrac{1}{2} \inf_{\psi_0 \in \Lambda(z)} \|\psi_0\|_C^2).
\end{aligned}
\qquad (21)
$$

It is clear from equation (18) that the stochastic sampling problem is replaced by a deterministic optimization problem, which we solve numerically as explained next. The trajectory initiated from the minimizer $\psi_0^\star$ of the action will be referred to as the *instanton trajectory*, and in the following we compare it to trajectories obtained from the experiment.

C. Numerical aspects

In practice, we perform the minimization (19) by numerical gradient descent in the space of the initial condition ψ_0, the gradient being computed by the adjoint formalism. Consequently, for each iteration of the descent, the NLSE (6) needs to be solved up to $x = L$ for the envelope ψ and its adjoint equation for the adjoint field $\tilde{\psi}$. The equation is solved in a time domain of width 75 s, much larger than the correlation time of the wave field (of the order of 10 seconds), with periodic boundary conditions in time. The domain is discretized on a lattice of 2^{11} equally spaced points. Combined with a cut-off of the initial spectrum at small amplitude, this leads to $M = 89$ modes of the JONSWAP being relevant for the initial data, as depicted in Fig. 2. Eq. (6) is numerically integrated in space by means of a pseudo-spectral exponential time-differencing method ETDRK2, with a spatial increment of 0.1 m. More details of the numerical procedure can be found in [26].

The minimizer $\psi_0^\star$ of (19) identifies the most likely realization over the distribution of wave shapes at the wave generator which, evolving deterministically via the NLSE, reaches a size $\eta(L,0) \geq z$. As saddle point approximation of the corresponding action, $\psi^\star(z)$ can be considered the *instanton* of the problem. Here, the large value of z plays the role of the limiting parameter for the LDP (18). Thus, the instanton of size z is expected to represent all of the extreme events $\eta(L,0) \geq z$ to leading order in z. Because of this key property, the instanton is the natural object for the characterization of the extreme wave events. Note that the knowledge of the instanton configuration itself can be used as an ingredient for advanced rare event sampling techniques, such as importance sampling and hybrid Monte Carlo approaches [51]. For the purpose of this paper, we restrict our analysis to the comparison of the instanton to the conditioned experimental measurements.

V. VALIDATION OF THE INSTANTON DESCRIPTION

In Fig. 4 we compare the evolution of rogue waves observed in the experiment and averaged over many realizations to that of the instanton, both constrained at $x = 45$ m. In all cases the instanton tracks the dynamics of the averaged wave very closely during the whole evolution. Moreover, in the focusing region the standard deviation around the mean is small, especially toward the end of the evolution. This observation in itself is a statement that indeed all of the rogue waves such that $\eta(L,0) \geq z$ resemble the instanton plus small random fluctuations. The instanton approximation shows excellent agreement not only across different degrees of nonlinearity (and therefore substantially different physical mechanisms), but also captures the behavior of precursors earlier along the channel.

In Fig. 5 the envelope evolution of a single realization of a rogue wave is compared to the instanton evolution at multiple locations, in the highly-nonlinear case. In the focusing region the experimental sample shares with the instanton the same overall structure, needed to allow it to reach an extreme size.

It is worth stressing that the instanton approach captures both the linear and the fully nonlinear cases, unlike previous theories that could describe each of these regimes individually but not both. To make that point, in the next two sections we compare the predictions of our approach to those of the quasi-determinism and semiclassical theories that hold in the dispersive and nonlinear regimes, respectively.

A. Comparison to linear theory

In the linear case, i.e. when the field $\psi(x,t)$ is Gaussian and stationary, the shape of an envelope time series with a large local maximum in $t = 0$ is expected to be given by the covariance of the wave field, i.e. the inverse
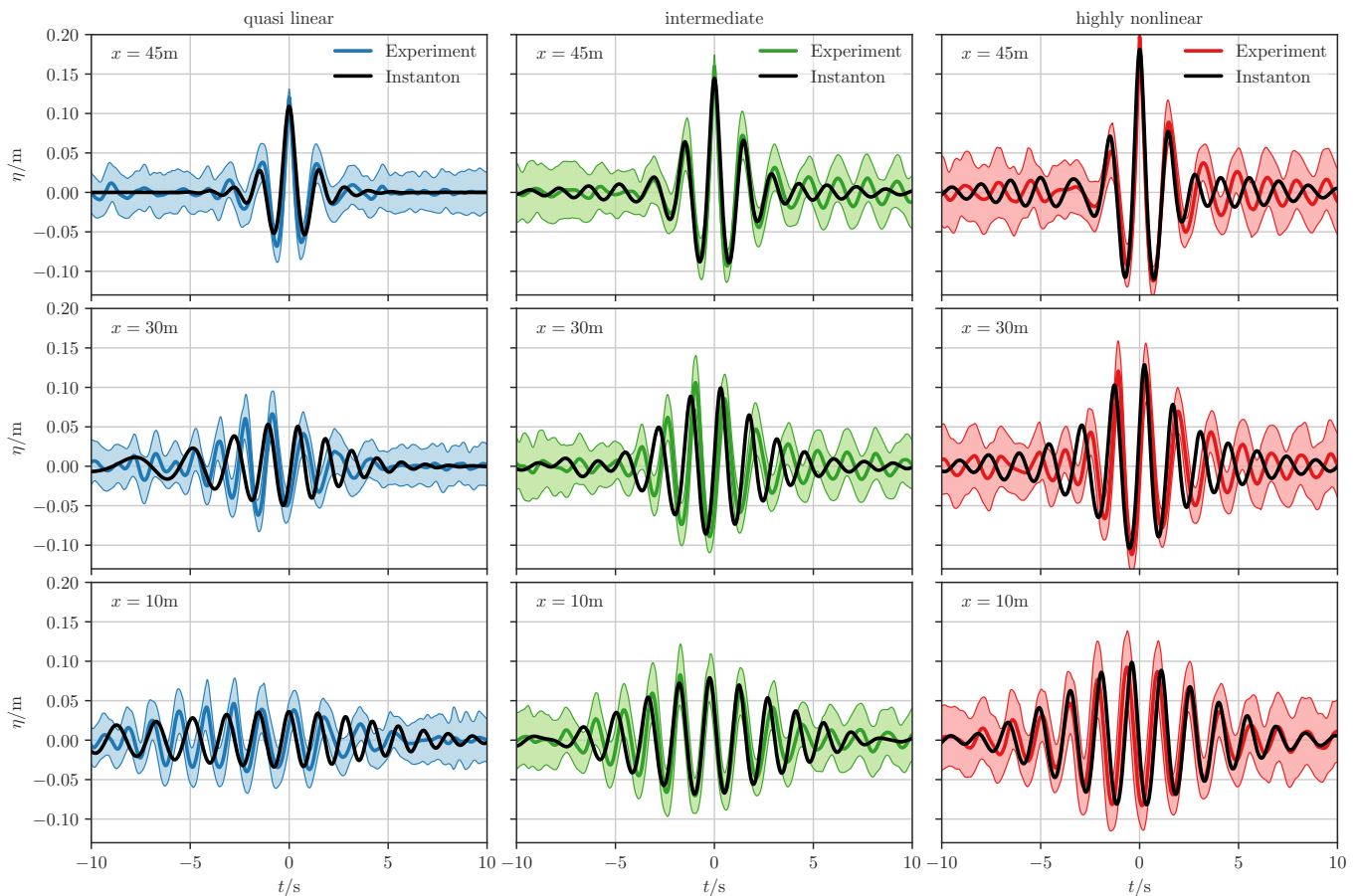
FIG. 4. Experimental validation of the instanton. Snapshots of the instanton during its evolution along the channel (black lines) are compared to the mean and standard deviation of the experimental rogue wave (color lines), for different regimes of nonlinearity. The instanton prediction agrees with the experimental mean across all regimes, and captures the whole evolution along the channel. This confirms that typical rogue waves are well represented by instantons, and the typical extreme events collapse onto this most likely one with only small fluctuations around them.

Fourier transform of the spectrum. This is a well established result in probability [17]. In the oceanographic context, the result was rediscovered in the '90s [18] and subsequently tested for some real quasi-Gaussian wave records in the ocean [52], also accounting for second-order Stokes' corrections [53]. A core result of the theory is the prediction that conditioning the surface elevation to have a large maximum, the expected shape of the water surface is given by the covariance of the wave field, i.e. the inverse Fourier transform of the spectrum. The theory is often referred to as the theory of quasi-determinism, which hereafter we name the linear theory for simplicity. In our case, such prediction is justified if the nonlinear focusing effects are small so that the statistics stay close to Gaussian along the tank, as in the quasi-linear set. Then, conditioning on a temporal maximum of $\eta(L, 0)$ at $x = L$, we can compute the history of the wave packet by evolving NLSE backward in space. In Fig. 6a this linear prediction is plotted in comparison with the envelope of the averaged rogue wave for the quasi-linear set. A good agreement is observed at all spatial points consid-

ered. Moreover, the theoretical instanton found through the optimization procedure reduces perfectly to the linear prediction, proving that such result is included in the instanton theory and represents its limiting linear case.

B. Nonlinear regime and Peregrine solitons

At the opposite end, in the nonlinear regime, it was recently shown [19] that in the zero-dispersion (semiclassical) regime of the NLSE any single localized pulse on a vanishing background leads locally to the emergence of a Peregrine soliton. By scale invariance of the NLSE, such a regime can be attained whenever an initial condition is characterized by large enough wave groups for which the nonlinear term dominates over the dispersive one. In fiber optics [54, 55], emerging Peregrine-like structures have been observed out of a random background. For the highly nonlinear case, in Fig. 6b we compare the instanton and the Peregrine soliton reaching the same maximal height z at $x = 45$ m, finding that in
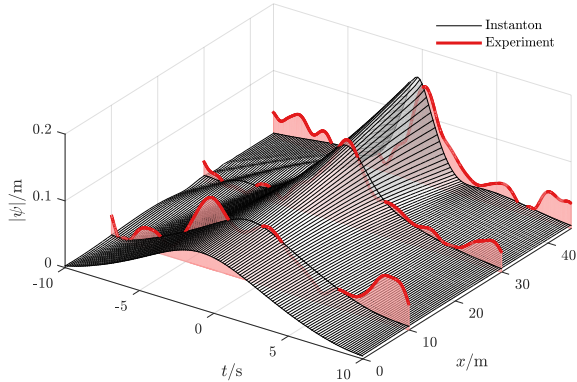
FIG. 5. Agreement of the instanton with individual extreme events. The evolution of a single realization of an extreme wave (red lines) is reasonably approximated by the instanton evolution (black/white surface), here for a sample of the highly nonlinear data set. In order to capture the focusing pattern in an essential way, the envelope $|\psi|$ is plotted instead of the surface elevation η to remove carrier-frequency oscillations.

the focusing region the two converge to the same shape, which is also closely followed by the envelope of the experimental averaged rogue wave. Looking at the event precursor at earlier x, instead, we notice that the experimental mean wave stays close to the instanton, while it gradually deviates from the Peregrine soliton. Thus, it appears that the instanton captures the mechanism underlying the rogue wave events also when nonlinearity rules over dispersion, tending locally to the Peregrine soliton around the maximal focusing point, consistently with the regularization of the gradient catastrophe [19].

C. A unified picture of rogue waves

A useful quantification of the effective mechanisms of rogue wave creation can be obtained by looking at the length scales at play. The linear length of dispersion is given by $L_{\text{lin}} = \omega_0^2/(k_0\Omega^2)$, while the characteristic length associated with the Peregrine soliton is $L_{\text{Per}} = \sqrt{L_{\text{lin}}L_{\text{nl}}}$ [44], where $L_{\text{nl}} = 8/(k_0^3 H_s^2)$ is the nonlinear length of modulational instability. These length scales are clearly visible in space-time contours of the amplitude shown in Fig. 6c, t. In the linear and quasi-linear regimes, the wave packet has a characteristic length around $L_{\text{lin}} \simeq 9$ m. Thus, we can state that linear superposition dominates and the expected mechanism leading to the extreme event is the linear dispersion of a coherent wave packet. The quasi-linear instanton evolution is almost indistinguishable from the linear approximation. On the other hand, the extent of the structures in the highly-nonlinear case agrees with the length $L_{\text{Per}} \simeq 65$ m. The dynamics of the highly nonlinear instanton clearly converges to the Peregrine dynamics near the space-time point of maxi-

mal focusing, and reproduces the characteristic isolated "dips" of the amplitude observed around the extreme event. Fig. 6c highlights the sharp difference between the rapidly evanescent linear rogue waves and the more persistent nonlinear ones. Quite strikingly, the instanton is able to interpolate between those two limiting regimes, as evidenced by the intermediate instanton in Fig. 6c, which displays features of both the linear theory and the Peregrine soliton. Summarizing, the instanton predicts the shape of rogue waves experimentally observed in the tank across all parameter regimes.

D. Probability estimates from LDT

The analysis so far has addressed the mechanism of rogue-wave formation, and compared the most likely evolution into an extreme wave, as predicted by the instanton, to the observed events measured in the experiment. Since the instanton formalism is based on probability theory and large deviations, it also allows us to deduce the tail scaling of the extreme event probability itself via (18). Indeed, it was shown in [50] that the LDT prediction for the tail of the PDFs match very well those obtained by brute-force Monte Carlo simulations using NLSE. In the context of actual experiments, the situation is more complicated. Despite the large amount of data collected in the experiments, the far tail of the PDF of the surface elevation is characterized by a natural cutoff related to the phenomenon of wave breaking, visually observed during the experiments in the non linear regimes. The NLSE itself misses such effect that lowers the probability to observe rogue wave in experiments, especially in the highly nonlinear regime. As a result, the predictions we can make about the PDFs of rogue waves are less accurate than those about their shape. In Fig. 7 we plot the LDT predictions for the PDF of the surface elevation, $\rho_L(z) = -P'_L(z)$, in the intermediate regime at three spatial points with $L = 10$, 30 and 45 m away from the wave maker, and compare them with the experimental ones. While the agreement is reasonable past the height threshold for rogue waves, and confirms the expected nonlinear tail fattening [36, 42], it is difficult to quantify how accurate these results are because of the problems mentioned earlier.

VI. CONCLUSIONS

Starting with the pioneering works in [56–58], it has been recognized that nonlinear focusing effects may play an important role in the formation of rogue waves. Since then, exact solutions of the NLSE, like for example the Peregrine solution, have been reproduced in controlled lab experiments [47, 59] and by now are considered as prototypes of rogue waves. In random wave fields, however, our understanding of the development of rogue waves remains more limited. In strongly nonlinear
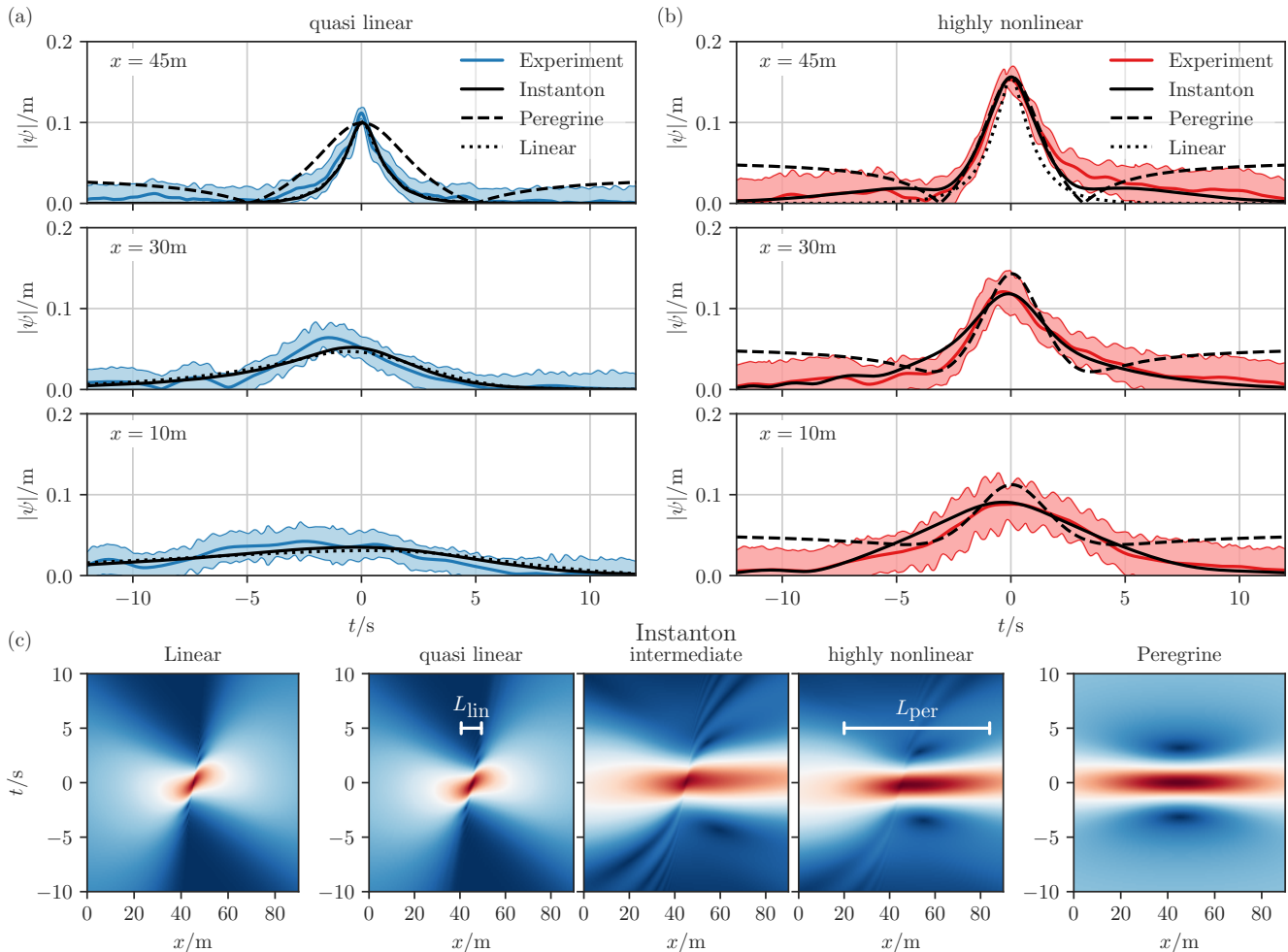
FIG. 6. Comparison of the instanton to the predictions of the theory of quasideterminism and the semiclassical theory: (a) The quasi-linear instanton converges to the linear prediction, correctly reproducing the rogue waves averaged over the experiments. (b) The highly nonlinear instanton evolution closely follows the averaged rogue wave and converges locally to a Peregrine soliton around its space-time maximum, as predicted by the semi-classical theory, and reproduced by the instanton. The linear prediction instead fails, especially around the maximum. (c) The contour plots show agreement with the two limiting theories and recover the respective dominant length scales. In the linear limit, dominated by dispersion, the rogue waves arise and decay very rapidly. On the contrary, in the semi-classical limit, where nonlinear effects are prevalent, the Peregrine-like structure of the extreme event is persistent, with a very slow decay. The rogue waves in intermediate regimes display both linear and nonlinear features, as shown in the central panel.

conditions (semiclassical limit), assuming a one dimensional propagation described by the NLSE, it has been shown [20] that a localized initial condition leads to the development of extreme waves that can be locally fitted to the Peregrine solution of the NLSE. While this fit may suggest the internal mechanism leading to rogue waves in long-crested, narrow-banded deep seas (neglecting other effects such as bathymetry, interactions with sea currents, multimodality, etc., which may also play a significant role in particular situations) it says nothing about their likelihood. Such information is instead intrinsically contained within the instanton framework, allowing for estimates such as in Fig. (7). To what extent these nonlinear effects are at work in real directional sea states is also a

difficult question [8, 9, 60], in part because of the uncertainty in the measurements of the directional wave spectrum, especially close to its peak. If the sea state conditions are not prone for the development of such nonlinear waves, linear dispersion may still be the dominant one for generating rogue waves [8]. This idea is at the core of the theory of quasi-determinism (also known as NewWave theory) that was developed in the early seventies to describe rogue waves in this linear regime [17, 18]; it allows one to determine the shape of the most extreme wave and relate it to the autocorrelation function. The two, apparently incompatible, mechanisms of formation of rogue waves, i.e. the nonlinear focusing and the linear superposition, have led to many debates among different
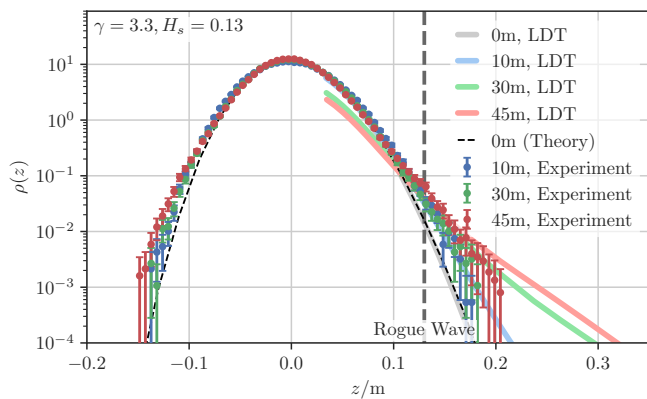
FIG. 7. Comparison of the PDF of the surface elevation $\rho(z) = -P'(z)$ obtained by binning the data from the experiments and the LDT estimates from Eq. (18), showing good agreement in the rogue-wave regime (right-hand side of the vertical dashed line, indicating the conventional Rogue wave threshold $z = H_s$). The figure refers to the intermediate regime. The blue, green and red colors indicate data collected at the probes 10, 30 and 45 m away from the wave maker, respectively.

groups of research.

Here we have proposed a unifying framework based on Large Deviation Theory and Instanton Calculus that is capable to describe with the same accuracy the shape of rogue waves that result either from a linear superposition or a nonlinear focusing mechanism. In the limit of large nonlinearity, the instantons closely resemble the Peregrine soliton used e.g. in [19, 20] to describe extreme events, but with the added bonus that our framework predicts their likelihood; in the limit of linear waves, the instanton reduces to the autocorrelation function as obtained in [17, 18]. A smooth transition between the two limiting regimes is also observed, and these predictions are fully supported by experiments performed in

a large wave tank with different degrees of nonlinearity. These results were obtained for one dimensional propagation, but there are no obstacles to apply the approach to two horizontal dimensions, which may finally explain the origin and shape of rogue waves in different setups, including the ocean.

VII. ACKNOWLEDGMENTS

Appendix A: Derivation of Eq. (9)

Let

$$\eta_0(t) = \tfrac{1}{2}\left(\psi_0(t)e^{-i\omega_0 t} + \bar{\psi}_0(t)e^{i\omega_0 t}\right), \qquad (A1)$$

then, using (8), this can also be written as

$$\eta_0(t) = \tfrac{1}{2}\int_{-\infty}^{\infty}\left(\hat{\psi}_0(\omega)e^{i(\omega-\omega_0)t} + \hat{\bar{\psi}}_0(\omega)e^{-i(\omega-\omega_0)t}\right)d\omega. \tag{A2}$$

This implies, using (9), that

$$\begin{aligned}\langle\eta(t)\eta(t')\rangle &= \tfrac{1}{2}\int_{-\infty}^{\infty}C(\omega-\omega_0)\cos((\omega-\omega_0)(t-t'))d\omega \\ &= \int_{0}^{\infty}C(\omega)\cos(\omega(t-t'))d\omega\end{aligned} \tag{A3}$$

which is consistent with (2).

[1] V. E. Zakharov, *Stability of periodic waves of finite amplitude on the surface of a deep fluid,* J. Appl. Mech. Tech. Phys. **9**, 190 (1968).

[2] M. Onorato, S. Residori, U. Bortolozzo, A. Montina, and F. Arecchi, *Rogue waves and their generating mechanisms in different physical contexts,* Phys. Rep. **528**, 47 (2013).

[3] N. Akhmediev, J. M. Dudley, D. Solli, and S. Turitsyn, *Recent progress in investigating optical rogue waves,* Journal of Optics **15**, 060201 (2013).

[4] H. Bailung, S. Sharma, and Y. Nakamura, *Observation of Peregrine solitons in a multicomponent plasma with negative ions,* Physical Review Letters **107**, 255005 (2011).

[5] C. Kharif, E. Pelinovsky, and A. Slunyaev, *Rogue waves in the ocean* (Springer Science & Business Media, 2008).

[6] M. Onorato, T. Waseda, A. Toffoli, L. Cavaleri, O. Gramstad, P. Janssen, T. Kinoshita, J. Monbaliu, N. Mori, A. R. Osborne, *et al.*, *Statistical properties of directional ocean waves: the role of the modulational instability in the formation of extreme events,* Physical Review Letters **102**, 114502 (2009).

[7] T. A. Adcock and P. H. Taylor, *The physics of anomalous ('rogue') ocean waves,* Reports on Progress in Physics **77**, 105901 (2014).

[8] F. Fedele, J. Brennan, S. P. De León, J. Dudley, and F. Dias, *Real world ocean rogue waves explained without the modulational instability,* Scientific reports **6**, 27715 (2016).

[9] A. Benetazzo, F. Ardhuin, F. Bergamasco, L. Cavaleri, P. V. Guimarães, M. Schwendeman, M. Sclavo, J. Thomson, and A. Torsello, *On the shape and likelihood of oceanic rogue waves,* Scientific Reports **7**, 8276 (2017).

[10] M. Onorato, A. R. Osborne, M. Serio, and S. Bertone, *Freak waves in random oceanic sea states,* Phys. Rev. Lett. **86**, 5831 (2001).

[11] R. Rajaraman, *Solitons and instantons: An Introduction to Solitons and Instantons in Quantum Field Theory*

(North Holland, 1982).

[12] M. I. Dykman, E. Mori, J. Ross, and P. Hunt, *Large fluctuations and optimal paths in chemical kinetics,* The Journal of Chemical Physics **100**, 5735 (1994).

[13] T. Schäfer and E. V. Shuryak, *Instantons in QCD,* Reviews of Modern Physics **70**, 323 (1998).

[14] G. Falkovich, I. Kolokolov, V. Lebedev, and A. Migdal, *Instantons and intermittency,* Physical Review E **54**, 4896 (1996).

[15] T. Grafke, R. Grauer, and T. Schäfer, *The instanton method and its numerical implementation in fluid mechanics,* Journal of Physics A: Mathematical and Theoretical **48**, 333001 (2015).

[16] T. Grafke, R. Grauer, T. Schäfer, and E. Vanden-Eijnden, *Relevance of instantons in Burgers turbulence,* EPL (Europhysics Letters) **109**, 34003 (2015).

[17] G. Lindgren, *Local maxima of Gaussian fields,* Arkiv för matematik **10**, 195 (1972).

[18] P. Boccotti, *Wave mechanics for ocean engineering*, Vol. 64 (Elsevier, 2000).

[19] M. Bertola and A. Tovbis, *Universality for the focusing nonlinear Schrödinger equation at the gradient catastrophe point: rational breathers and poles of the tritronquée solution to Painlevé I,* Communications on Pure and Applied Mathematics **66**, 678 (2013).

[20] A. Tikan, C. Billet, G. El, A. Tovbis, M. Bertola, T. Sylvestre, F. Gustave, S. Randoux, G. Genty, P. Suret, *et al.*, *Universality of the Peregrine soliton in the focusing dynamics of the cubic nonlinear Schrödinger equation,* Physical Review Letters **119**, 033901 (2017).

[21] A. AghaKouchak, D. Easterling, K. Hsu, S. Schubert, and S. Sorooshian, *Extremes in a changing climate: detection, analysis and uncertainty*, Vol. 65 (Springer Science & Business Media, 2012).

[22] D. Coumou and S. Rahmstorf, *A decade of weather extremes,* Nature climate change **2**, 491 (2012).

[23] C. B. Field, V. Barros, T. F. Stocker, and Q. Dahe, *Managing the risks of extreme events and disasters to advance climate change adaptation: special report of the intergovernmental panel on climate change* (Cambridge University Press, 2012).

[24] T. G. Shepherd, *A common framework for approaches to extreme event attribution,* Current Climate Change Reports **2**, 28 (2016).

[25] M. A. Mohamad, W. Cousins, and T. P. Sapsis, *A probabilistic decomposition-synthesis method for the quantification of rare events due to internal instabilities,* J. Comp. Phys. **322**, 288 (2016).

[26] G. Dematteis, T. Grafke, and E. Vanden-Eijnden, *Extreme event quantification in dynamical systems with random components,* SIAM/ASA Journal on Uncertainty Quantification **7**, 1029 (2019).

[27] P. Glasserman, P. Heidelberger, P. Shahabuddin, and T. Zajic, *Multilevel splitting for estimating rare event probabilities,* Operations Research **47**, 585 (1999).

[28] S. Juneja and P. Shahabuddin, *Rare-event simulation techniques: an introduction and recent advances,* Handbooks in operations research and management science **13**, 291 (2006).

[29] F. Cérou and A. Guyader, *Adaptive multilevel splitting for rare event analysis,* Stochastic Analysis and Applications **25**, 417 (2007).

[30] C. Giardina, J. Kurchan, V. Lecomte, and J. Tailleur, *Simulating rare events in dynamical processes,* Journal of statistical physics **145**, 787 (2011).

[31] J. Tailleur and J. Kurchan, *Probing rare physical trajectories with Lyapunov weighted dynamics,* Nature Physics **3**, 203 (2007).

[32] E. Vanden-Eijnden and J. Weare, *Rare Event Simulation of Small Noise Diffusions,* Communications on Pure and Applied Mathematics **65**, 1770 (2012).

[33] M. Farazmand and T. P. Sapsis, *A variational approach to probing extreme events in turbulent dynamical systems,* Science Advances **3**, e1701533 (2017).

[34] F. Ragone, J. Wouters, and F. Bouchet, *Computation of extreme heat waves in climate models using a large deviation algorithm,* Proceedings of the National Academy of Sciences , 201712645 (2017).

[35] M. Onorato, A. Osborne, R. Fedele, and M. Serio, *Landau damping and coherent structures in narrow-banded 1+ 1 deep water gravity waves,* Physical Review E **67**, 046305 (2003).

[36] M. Onorato, A. R. Osborne, M. Serio, and L. Cavaleri, *Modulational instability and non-Gaussian statistics in experimental random water-wave trains,* Physics of Fluids **17**, 078101 (2005).

[37] I. Alber, *The effects of randomness on the stability of two-dimensional surface wave trains,* Proceedings of the Royal Society of London. A. Mathematical and Physical Sciences **363**, 525 (1978).

[38] M. Stiassnie, A. Regev, and Y. Agnon, *Recurrent solutions of alber's equation for random water-wave fields,* Journal of Fluid Mechanics **598**, 245 (2008).

[39] A. Ribal, A. V. Babanin, I. Young, A. Toffoli, and M. Stiassnie, *Recurrent solutions of the alber equation initialized by joint north sea wave project spectra,* Journal of Fluid Mechanics **719**, 314 (2013).

[40] O. Gramstad, *Modulational instability in jonswap sea states using the alber equation,* in *ASME 2017 36th International Conference on Ocean, Offshore and Arctic Engineering* (American Society of Mechanical Engineers, 2017) pp. V07BT06A051–V07BT06A051.

[41] A. Athanassoulis, G. Athanassoulis, and T. Sapsis, *Localized instabilities of the wigner equation as a model for the emergence of rogue waves,* Journal of Ocean Engineering and Marine Energy **3**, 353 (2017).

[42] M. Onorato, A. R. Osborne, M. Serio, L. Cavaleri, C. Brandini, and C. T. Stansberg, *Extreme waves, modulational instability and second order theory: wave flume experiments on irregular waves,* European Journal of Mechanics-B/Fluids **25**, 586 (2006).

[43] K. Hasselmann, T. P. Barnett, E. Bouws, H. Carlson, D. E. Cartwright, K. Enke, J. A. Ewing, H. Gienapp, D. E. Hasselmann, P. Kruseman, *et al.*, *Measurements of wind-wave growth and swell decay during the Joint North Sea Wave Project (JONSWAP)*, Tech. Rep. (Deutsches Hydrographisches Institut, 1973).

[44] R. El Koussaifi, A. Tikan, A. Toffoli, S. Randoux, P. Suret, and M. Onorato, *Spontaneous emergence of rogue waves in partially coherent waves: a quantitative experimental comparison between hydrodynamics and optics,* Physical Review E **97**, 012208 (2018).

[45] T. B. Benjamin and J. E. Feir, *The disintegration of wave trains on deep water Part 1. Theory,* J. Fluid Mech. **27**, 417 (1967).

[46] N. Akhmediev, J. M. Soto-Crespo, and A. Ankiewicz, *Extreme waves that appear from nowhere: on the nature of rogue waves,* Physics Letters A **373**, 2137 (2009).

[47] A. Chabchoub, N. Hoffmann, and N. Akhmediev, *Rogue wave observation in a water wave tank,* Phys. Rev. Lett. **106**, 204502 (2011).

[48] K. Trulsen, I. Kliakhandler, K. B. Dysthe, and M. G. Velarde, *On weakly nonlinear modulation of waves on deep water,* Physics of Fluids (1994-present) **12**, 2432 (2000).

[49] O. Gramstad and K. Trulsen, *Hamiltonian form of the modified nonlinear schrödinger equation for gravity waves on arbitrary depth,* J. Fluid Mech. **670**, 404 (2011).

[50] G. Dematteis, T. Grafke, and E. Vanden-Eijnden, *Rogue waves and large deviations in deep sea,* Proceedings of the National Academy of Sciences , 201710670 (2018).

[51] G. Margazoglou, L. Biferale, R. Grauer, K. Jansen, D. Mesterhzy, T. Rosenow, and R. Tripiccione, *Hybrid Monte Carlo algorithm for sampling rare events in space-time histories of stochastic fields,* Physical Review E **99**, 053303 (2019).

[52] M. A. Tayfun and F. Fedele, *Expected shape of extreme waves in storm seas,* in *ASME 2007 26th International Conference on Offshore Mechanics and Arctic Engineering* (American Society of Mechanical Engineers, 2007) pp. 53–60.

[53] F. Fedele and F. Arena, *Weakly nonlinear statistics of high random waves,* Physics of fluids **17**, 026601 (2005).

[54] P. Suret, R. El Koussaifi, A. Tikan, C. Evain, S. Randoux, C. Szwaj, and S. Bielawski, *Single-shot observation of optical rogue waves in integrable turbulence using time microscopy,* Nature communications **7**, 13136 (2016).

[55] A. Tikan, *Effect of local Peregrine soliton emergence on statistics of random waves in the 1-d focusing nonlinear Schrödinger equation,* arXiv preprint arXiv:1905.11938 (2019).

[56] K. B. Dysthe and K. Trulsen, *Note on breather type solutions of the NLS as models for freak-waves,* Physica Scripta **T82**, 48 (1999).

[57] K. Henderson, D. Peregrine, and J. Dold, *Unsteady water wave modulations: fully nonlinear solutions and comparison with the nonlinear Schrödinger equation,* Wave Motion **29**, 341 (1999).

[58] A. Osborne, M. Onorato, and M. Serio, *The nonlinear dynamics of rogue waves and holes in deep–water gravity wave train,* Phys. Lett. A **275**, 386 (2000).

[59] B. Kibler, J. Fatome, C. Finot, G. Millot, F. Dias, G. Genty, N. Akhmediev, and J. M. Dudley, *The Peregrine soliton in nonlinear fibre optics,* Nature Physics **6**, 790 (2010).

[60] M. Onorato, T. Waseda, A. Toffoli, L. Cavaleri, O. Gramstad, P. Janssen, T. Kinoshita, J. Monbaliu, N. Mori, A. R. Osborne, *et al.*, *Statistical properties of directional ocean waves: the role of the modulational instability in the formation of extreme events,* Phys. Rev. Lett. **102**, 114502 (2009).